

Structures and Electronic Properties of Different $\text{ZnIn}_2\text{S}_4/\text{CuInS}_2$ Interface: A First-Principles Study

Yao Wang, Xiao-Nan Wei, Tian-Yu Tang, Qi Dai, Zhi-Qiao Chen and Yan-Lin Tang*

School of Physics, Guizhou University, Guiyang 550025, China

Abstract: This paper aims to explore the electronic and photoelectric properties of two-dimensional type I (straddle) heterojunctions by theoretical calculation, and to provide theoretical support for the design of novel optoelectronic devices. Several $\text{ZnIn}_2\text{S}_4/\text{CuInS}_2$ two-dimensional type I heterojunctions with different terminations have been systematically investigated by density functional theory (DFT) combined with tight binding approximation. The results show that only two of these structures are stable. In these two stable structures, different chemical bonds and electron transfer directions are formed when different atoms are exposed at the interface. The calculation results of band structures show that both of these structures are two-dimensional type I heterojunctions. The calculation results of effective mass show that they have efficient carrier separation and transport characteristics. These properties indicate that these two heterostructures can be used in high-performance light-emitting devices and photoelectric sensors. This study provides a theoretical basis for the optimal design of new two-dimensional optoelectronic devices.

Keyword: First principles calculation, ZnIn_2S_4 , CuInS_2 , Heterojunction.

INTRODUCTION

In recent years, many breakthrough achievements have been made in the fields of high-performance light-emitting devices and photoelectric sensors, injecting new impetus into the development of science and technology. Among them, research teams from the University of Science and Technology of China and others have achieved a major breakthrough in quantum dot light-emitting diode (QLED) technology. They successfully guided the quantum dots to achieve efficient arrangement by ingeniously utilizing the dipole-dipole interaction in the mixed-phase CdZn SeS quantum dots. This innovative measure has significantly enhanced the photon external coupling efficiency in light-emitting diodes, raising the external quantum efficiency of quantum dot LEDs to 35.6% in one go. At the same time, it demonstrates extremely high stability, laying a solid foundation for the commercial application of QLEDs. In the field of organic electroluminescent devices (OLEDs), researchers have also achieved remarkable results. They effectively enhanced the efficiency and stability of OLEDs by meticulously designing innovative structures such as stacked light-emitting layer structures and multi-quantum well structures. Taking the stacked light-emitting layer structure as an example, this structure can ingeniously promote the diffusion of triplet excitons generated in the region with a high doping concentration of phosphorescent dyes to the adjacent region with a low doping concentration of phosphorescent dyes, thereby reducing the aggregation of triplet excitons, suppressing the quenching phenomenon of triplet excitons, and significantly improving the overall performance of

OLEDs. In the field of photoelectric sensors, MEMS technology has undoubtedly become the core force driving the miniaturization revolution. With the continuous improvement of manufacturing technology, the size of photoelectric sensors is constantly shrinking, and at the same time, their functional integration is steadily increasing. Nowadays, a single sensor can integrate more functions to adapt to various complex and changeable application scenarios. For instance, the multi-spectral sensor equipped in the Huawei Mate70 series and the flexible pressure sensor adopted in the Xiaomi smart glasses are both fabricated based on advanced MEMS technology, achieving a leap in performance. These remarkable research advancements not only powerfully promote the rapid development of related technologies but also open up vast and boundless space for future technological applications. Although significant achievements have been made in the development of high-performance light-emitting devices and photoelectric sensors, many challenges are also faced, such as: quantum efficiency and light decay, material stability, defect control, cost and environmental friendliness. Solving these problems has become an important research area in materials physics. The construction of two-dimensional (2D) type I heterojunctions can provide an effective way to solve these problems.

Two-dimensional (2D) type I heterostructure refers to the heterostructure formed by two semiconductor materials, the conduction band and valence band are bent, resulting in electrons and holes are bound in the slit region of the heterostructure. Such structures usually have strong light absorption capacity and efficient carrier separation and transport characteristics [1]. Therefore, Type 2D I heterostructures, through their unique band structure and carrier dynamics,

*Address correspondence to this author at the School of Physics, Guizhou University, Guiyang 550025, China; E-mail: tylgzu@163.com

provide a powerful tool for solving challenges in high-performance light-emitting devices and photoelectric sensors.

ZnIn₂S₄ is a ternary metal sulfide, which has been widely used in various fields due to its advantages such as suitable band gap, non-toxic and easy preparation [2-9]. In the field of photocatalysis: Researchers can achieve better photocatalytic performance by designing its morphology and structure, and implementing modulation strategies such as vacancy engineering and doping engineering. For instance, highlighting the Pt unit point on the hexagonal ZnIn₂S₄ can accelerate photocatalytic hydrogen evolution, significantly increasing the hydrogen evolution rate; In the field of electronic devices: ZnIn₂S₄ has a high electrical conductivity and good thermal stability, and can be used as a semiconductor material to prepare electronic devices such as field-effect transistors and solar cells; In the field of energy conversion: ZnIn₂S₄ can also be used in piezoelectric conversion devices to convert mechanical energy into electrical energy; In the field of batteries: ZnIn₂S₄ can be used in lithium-sulfur batteries as a catalyst to promote the REDOX reaction of sulfur. For instance, the series REDOX reaction of S₈ and Li₂S was achieved through the sandwich structure of ZnIn₂S₄-In₂O₃-ZnIn₂S₄, enhancing the rate capacity, cycle stability and high area capacity of lithium-sulfur batteries, etc. However, the rapid recombination of its photogenic vectors has hindered its further application. To solve this problem, it needs to be coupled to other semiconductor materials. Therefore, the construction of a novel layered core-shell composite photocatalytic material which can effectively promote the separation and transport of photogenerated charge is the focus of current research. For example, Feng *et al.* constructed a 1D/2D CoS_{1.097}@ZnIn₂S₄ heterostructure. This unique structure can improve the utilization rate of visible light spectrum, provide more sites for photoelectron-hole separation and transport, improve the separation and transport efficiency of photoelectron-hole separation and transport. At the same time, the material also has good hydrogen evolution performance [10]. Tan *et al.* constructed the MIL-68(In)@ZnIn₂S₄ heterostructure to reduce the charge transfer resistance of high-performance photocatalytic hydrogen evolution [11]. The Z-type TiO_{2-x}@ZnIn₂S₄ heterojunction photocatalyst discovered by Zhang *et al.* can achieve the visible light photocatalytic oxidation of TC and tofuranoin. This new photocatalytic material has good performance of photogenerated carrier separation and transport [12]. In addition to metal oxides and sulfides, CdIn₂S₄, as an alternative ternary metal sulfide, has attracted much attention due to its application in the preparation of heterojunctions with ZnIn₂S₄, which aims to improve the separation efficiency of photogenerated charges.

Copper indium sulfide (CuInS₂) stands out as a quintessential P-type semiconductor, characterized by its minuscule band gap, approximately 1.45 eV, and exceptional capability for capturing light [13, 14]. It has piqued the curiosity of numerous scholars within the sphere of material science. Take, for instance, the creation of a CuInS₂/m-BiVO₄ photocatalyst featuring p-n heterojunctions by Kaowphong and his research team [15]. The accelerator demonstrated proficient surface charge transfer capabilities during the photo-decomposition of colored organic compounds and the neutralization of microbial entities, showcasing outstanding performance.

Despite the fact that p-n junction semiconductor recombination processes can boost the division of electron-hole pairs, the oxidative-reductive potential for the photo-produced electrons and holes remains constrained. The conventional type II heterojunction is capable of accomplishing charge carrier segregation solely within a spatial context, and its capacity for enhancing catalytic efficacy is constrained. The innovative S-scheme heterojunction architecture enhances the movement of photogenerated charge carriers, maintaining the robust REDOX capabilities of the electron-hole pairs. The research team led by Wang employed a solvothermal process to fabricate CuInS₂ nanosheets directly onto WO₃ nanoplates, creating an S-scheme hybrid catalyst that significantly accelerated the photofenton process for the elimination of TC from aquatic resources. The research team led by Guan crafted an innovative 2D/2D hybrid CuInS₂/ZnIn₂S₄ nanoscale sheet to enhance the process of hydrogen generation via solar energy [16]. The analysis of the structure reveals that the CuInS₂/ZnIn₂S₄ two-dimensional heterojunction, featuring a compatible lattice structure, is constructed from minute nanoscale sheets that exhibit an extensive area of interface contact. This configuration facilitates enhanced charge migration and partitioning. The utilization of 2D/2D phase heterogeneity offers a promising strategy for markedly enhancing the efficiency of solar hydrogen generation utilizing ZnIn₂S₄. Xiang and his colleagues developed an innovative S-scheme heterojunction structure composed of CuInS₂ and ZnIn₂S₄ (denoted as CIS/ZIS) through a one-pot solvothermal synthesis approach [17]. The results showed that the photocatalytic removal rates of antibiotics and Cr(VI) were significantly improved by CIS/ZIS heteroconjugate, and the removal rates of tetracycline (TC) (20 mg/L) and Cr(VI) (20 mg/L) were both above 90% under visible light irradiation. Bozhko *et al.* prepared CuInS₂-ZnIn₂S₄ solid alloys by liquid deposition and investigated the temperature dependence of their conductivity and thermal stimulation current in the temperature range of 27-300

K. Their photoconductive spectrum distribution was analyzed at $t \sim 30\text{k}$. The results show that induced light conduction is observed in the crystal [18]. Li *et al.* successfully prepared $\text{CuInS}_2/\text{ZnIn}_2\text{S}_4$ heterojunction with Z-type structure by hydrothermal synthesis method. The structural characterization shows that the interfacial contact area of $\text{CuInS}_2/\text{ZnIn}_2\text{S}_4$ heterojunction with lattice matching is increased, which is favorable for photogenic charge transfer and separation. Minute examination reveals that the $\text{CuInS}_2/\text{ZnIn}_2\text{S}_4$ amalgam boasts an intricately intertwined boundary and assumes a shape reminiscent of a diminutive sugar cube. The spectral analysis via photochemical means reveals that the utilization of a heterojunction configuration significantly enhances the capture of visible light and the efficacy of charge separation, thereby boosting the photocatalytic performance. The research indicates that the $\text{CuInS}_2/\text{ZnIn}_2\text{S}_4$ heterojunction photocatalyst with a Z-scheme configuration demonstrates improved hydrogen generation performance, offering an effective structural blueprint for harnessing solar energy to produce hydrogen as a fuel. Therefore, this heterojunction photocatalyst has a good application prospect in solar hydrogen production [19].

In addition, CuInS_2 can also be combined with ZnIn_2S_4 to form a 2D type I $\text{ZnIn}_2\text{S}_4/\text{CuInS}_2$ heterostructure, which can effectively solve the problems faced by high-performance light-emitting devices and photoelectric sensors. In this study, several $\text{ZnIn}_2\text{S}_4/\text{CuInS}_2$ two-dimensional type I heterostructures with different terminations are systematically studied by using density functional theory (DFT) combined with tight binding approximation. The structural stability, interfacial

electron transfer properties, band structure and effective mass are calculated, and the specific calculation process is as follows.

2. COMPUTATIONAL METHODS

This paper adopts the first principles calculation Simulation software VASP (Vienna Ab-initio Simulation Package) based on density functional theory [20-22]. The OTFG Ultrasoft pseudo-potential was adopted to treat the electron-ion interactions, while the generalized gradient approximation (GGA) with the scheme of Perdew-Burke-Ernzerhof (PBE) was applied to dispose the exchange-correlation term [23]. The zero damping DFT-D3 method of Grimme is used to correct the van der Waals forces between layers. All K grid points in Brillouin region are selected to be $5 \times 5 \times 1$, and the plane wave truncation energy is set to 400 eV, and all atoms in the cell are completely relaxed. The convergence accuracy of relaxation is set to 2×10^{-5} eV/atom. The calculated lattice constants of CuInS_2 are $a = 5.52\text{\AA}$, $b = 5.52\text{\AA}$, $c = 11.11\text{\AA}$, which are close to the experimental values [24]. The lattice constants of ZnIn_2S_4 are $a = 10.63\text{\AA}$, $b = 10.63\text{\AA}$, and $c = 10.63\text{\AA}$, which are close to the experimental values. This shows that our calculation method is reliable. Because the lattice mismatch between CuInS_2 's section and ZnIn_2S_4 's section is to be less than 5%, this study mainly considers six different interface heterostructures constructed between CuInS_2 's (100) (010) (100) surface and ZnIn_2S_4 's (001) (010) surface. By surface energy testing, the four-layer CuInS_2 structure and the four-layer ZnIn_2S_4 structure are sufficient to calculate the properties of the constructed heterojunction. Of the six structures built, only two are stable, and the optimized structure model is shown in Figure 1.

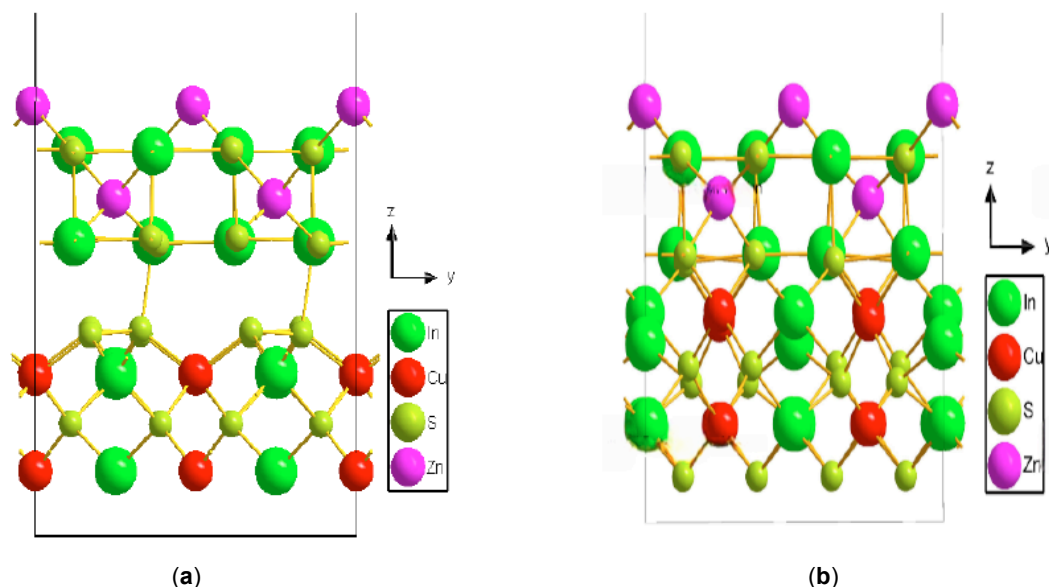


Figure 1: Two stable structures after optimization.

3. RESULTS AND DISCUSSION

3.1. Structure Stability

Binding Energy, also known as cohesion energy, refers to the energy required to pull atoms (or ions, or molecules) in a crystal from their equilibrium position to infinity (or the crystal surface) [25, 26]. Or you can think of it as the energy released when you combine free atoms into crystals. In simulation calculations, the stability of different structures can be compared by calculating their binding energies. Generally, when the associative energy is negative, it means that the structure is stable, and when the associative power registers a positive value, it indicates that the configuration is susceptible to change. Conversely, a structure exhibits enhanced stability as the binding energy dips further into the negative range. The formula for calculating binding energy is:

$$E_b = E_{total} - E_C - E_z \quad (1)$$

where, E_b represents the binding energy of the structure, E_{total} represents the total energy of the ZnIn₂S₄/CuInS₂ heterostructure, E_C and E_z represent the energy of the isolated CuInS₂ and ZnIn₂S₄ system after full relaxation. The binding energies of the six structures constructed were calculated, and the calculation results were shown in Table 1. The results show that the binding energy of only a and b of the six structures is negative, while that of the remaining four structures is positive. According to the definition of binding energy, it is evident that a structure exhibits stability when its binding energy drops below zero, whereas an unstable structure is indicated by a binding energy that surpasses zero. Additionally, a lower binding energy signifies a higher degree of stability for the structure. The binding energy of structure a is

-1.05eV, and that of structure b is -4.47eV. Therefore, of the six structural models constructed, only two structures, a and b, are stable, and structure b is more stable than structure a. Therefore, in the following research, we mainly study the electronic properties of these two stable structures.

3.2. Interfacial Electronic Properties

3.2.1. Work Function

The threshold energy necessary for electrons to break free from the metallic interior and reach the vacuum state is termed the work function [27], typically equating to roughly half the energy needed to ionize the metal's isolated atoms. This value of the work function indicates the degree of electron binding within the metal, with higher values signifying greater resistance for electrons to the metallic surface. The work function is calculated as follows:

$$W = -e\varphi - E_{Fermi} \quad (2)$$

where, $-e\varphi$ is the energy of the electrons at rest in the vacuum near the surface, E_{Fermi} is the electrostatic potential energy. It's Fermi energy. W is the work function. The work functions of heterostructure a and b are shown in Table 2.

The computed work function values indicate the formation of an internal electric field at the junction between CuInS₂ and ZnIn₂S₄, and the electron transfer at the interface of ZnIn₂S₄/CuInS₂ heterogeneous structure can be determined by the value of the work function. For heterostructure a, the work function of the CuInS₂ material is 5.23 eV, and the work function of the ZnIn₂S₄ material is 4.45 eV, so for heterostructure a, electrons flow from ZnIn₂S₄ material to the CuInS₂ material at the interface. For heterostructure b, the

Table 1: Binding Energy of Six Structures

	Section (CuInS ₂ /ZnIn ₂ S ₄)	Lattice Mismatch Rate	Binding Energy (eV)
a	(100)/(001)	3.87%	-1.05
b	(100)/(010)	4.47%	-4.47
c	(001)/(001)	3.87%	8.03
d	(001)/(010)	3.87%	3.91
e	(010)/(010)	4.47%	3.91
f	(110)/(011)	4.47%	1.62

Table 2: The Work Function of Structures a and b

Structure	a		b	
	CuInS ₂	ZnIn ₂ S ₄	CuInS ₂	ZnIn ₂ S ₄
W(eV)	5.23	4.45	5.31	5.41

work function of the CuInS_2 material is 5.31 eV, and the work function of the ZnIn_2S_4 material is 4.45 eV, so for heterostructure b, electrons flow from the CuInS_2 material to the ZnIn_2S_4 material at the interface.

The results of work function calculation show that the internal electric field is generated at the interface of $\text{ZnIn}_2\text{S}_4/\text{CuInS}_2$ heterostructure and the direction of electron transfer of heterostructure a at the interface is different from that of heterostructure b.

3.2.2. Differential Charge Density and Electron Localization Function

The calculation of the work function can determine whether an internal electric field is generated at the interface of the heterostructure and the direction of electron transfer at the interface. The differential charge density and electron localization function can help us understand more clearly at the microscopic level the electron transfer direction, bonding type, search for catalytic reaction active sites and material surface adsorption sites at the interface of heterogeneous structures, etc. The specific

introduction of differential charge density and electron local function is as follows:

The charge density difference [28-30] pertains to the variation in charge density following the bonding process as opposed to the charge density of the atomic structure at that particular location. It is one of the important indexes of electronic structure and chemical reaction of materials. By meticulously evaluating the differential charge distribution, it is feasible to discern the migration of charges and the orientation of polarization in the bonds during the interaction of bonding electrons with other bonding electrons. Differential charge density can reflect the polarity of chemical bond, reactivity and distribution of electron cloud, which is of great significance for studying the electronic structure and chemical reaction of materials.

Electron Localization Function (ELF) [31-34] serves as a technique for examining the electronic configuration. This approach is employed to depict the likelihood of encountering an electron with matching spin in proximity to another electron situated at a

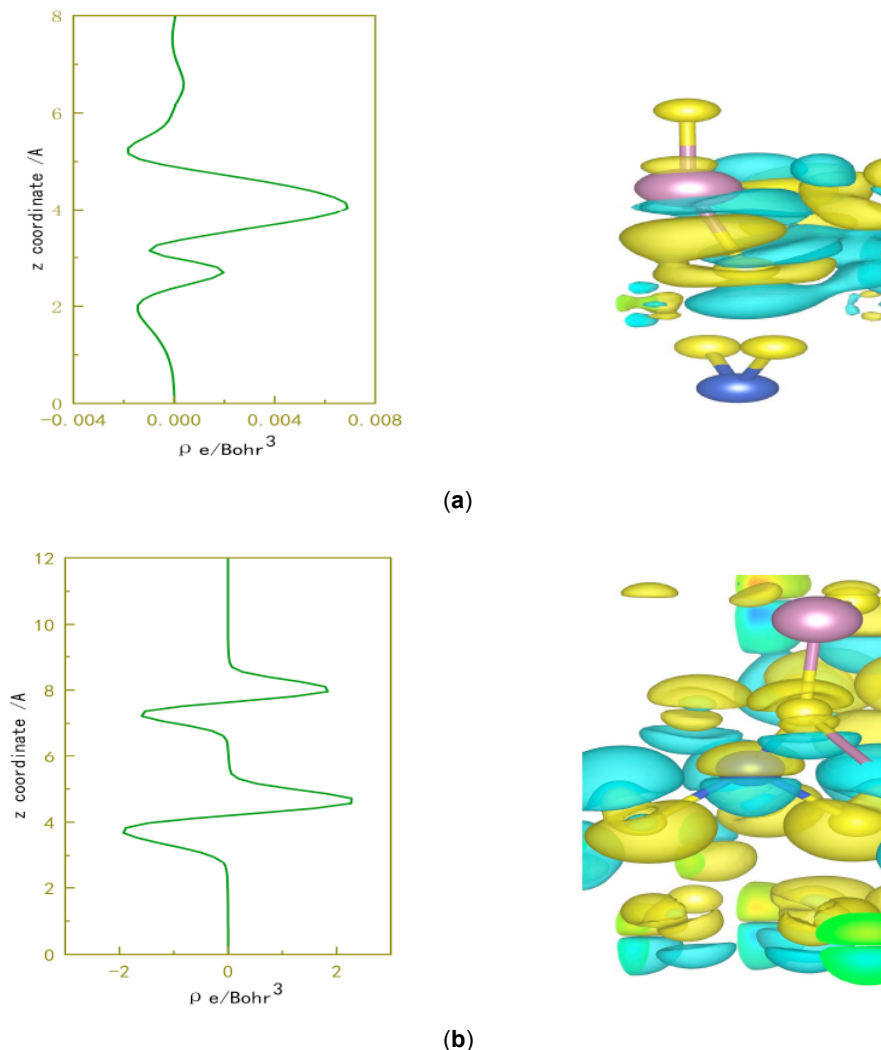


Figure 2: Differential charge-density maps of structures a and b (yellow for electrons, cyan for electrons lost).

designated spot, functioning as a benchmark. It quantifies the extent of localization for the benchmark electron and also provides a means to illustrate the probability distribution of electron pairs within a system containing multiple electrons. ELF ranges from 0 to 1, with $\text{ELF}=1$ indicating complete localization of the electron, shown in red. $\text{ELF}=0.5$ corresponds to the pairwise probability of the electron-like gas type, shown in yellow. $\text{ELF}=0$ represents the complete delocalization of the electron, shown in blue. This function can effectively analyze the degree of electron localization, such as the analysis of the electron shell configuration of heavy elements. In molecules, ELF can clearly distinguish the nuclear and valence states, and can also show covalent bonds and unshared electron pairs.

In order to further study the electron transfer at the $\text{ZnIn}_2\text{S}_4/\text{CuInS}_2$ heterostructural interface and whether chemical interaction or van der Waals interaction occurs at the heterostructural interface, the differential charge density and electron localization function of the two structures were calculated, as shown in Figure 2 and Figure 3. From the calculation results, it can be seen that for structure a, In in ZnIn_2S_4 in the upper structure loses electrons, while S in CuInS_2 in the lower structure gains electrons. When the contour line of the electron localization function is 0.85, it can be seen from the electron localization function diagram that the electron localization is around the S atom, and when the value of the contour line is changed, the electron still resides firmly around the S atom. For structure b, Cu and In in the lower CuInS_2 structure lose electrons, while S in ZnIn_2S_4 above gains electrons. When the contour line of the electron localization function is 0.85, it can be seen from the electron localization function

diagram that the electron localization is around the S atom, and when the value of the contour line is changed, the electron still resides firmly around the S atom.

3.2.3. Bader Charge Population Analysis

Bader charge population [35-37] analysis is a topology-based method for calculating the charge distribution of atoms in a molecule or solid. This method, developed by Richard F.W. Bader, defines the volume of an atom by identifying the zero-flux plane of the charge density and assigning the charge within these volumes to the corresponding atom. Bader charge analysis can provide important information about the transfer and localization of electrons between atoms [38, 39], which is very useful in materials science and chemistry.

The work function, differential charge density and electron local function are all qualitative analyses of electron transfer at the interface of heterogeneous structures. When the electron transfer at the interface is very complicated, it cannot be analyzed effectively by calculating the differential charge density and electron local function. The Bader charge layout analysis can quantitatively analyze the charge transfer at the interface of heterogeneous structures. In this study, Bader charge analysis was performed on some atoms at the interface, shown in Figure 4. The calculation results show that for heterostructure a, the In atom in ZnIn_2S_4 material lost electrons, and a part of its lost electrons were transferred to the S atom in ZnIn_2S_4 , while the other part of electrons were likely transferred to the S atom in CuInS_2 material. As for heterostructure b, it can be seen from the Bader charge that the In atom in ZnIn_2S_4 loses electrons, and some of the lost

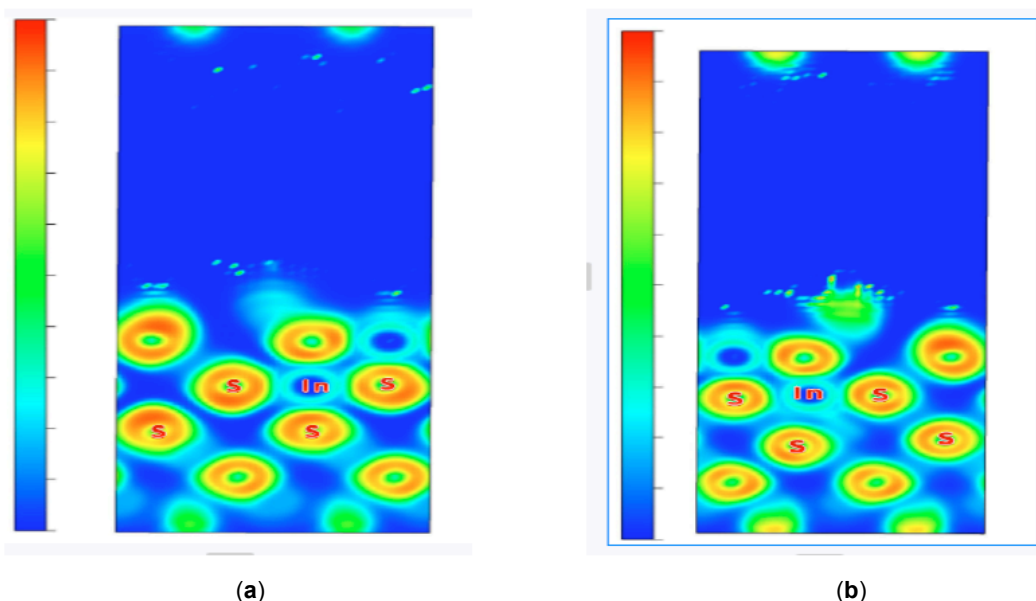


Figure 3: Electron local function diagram of structure a and b.

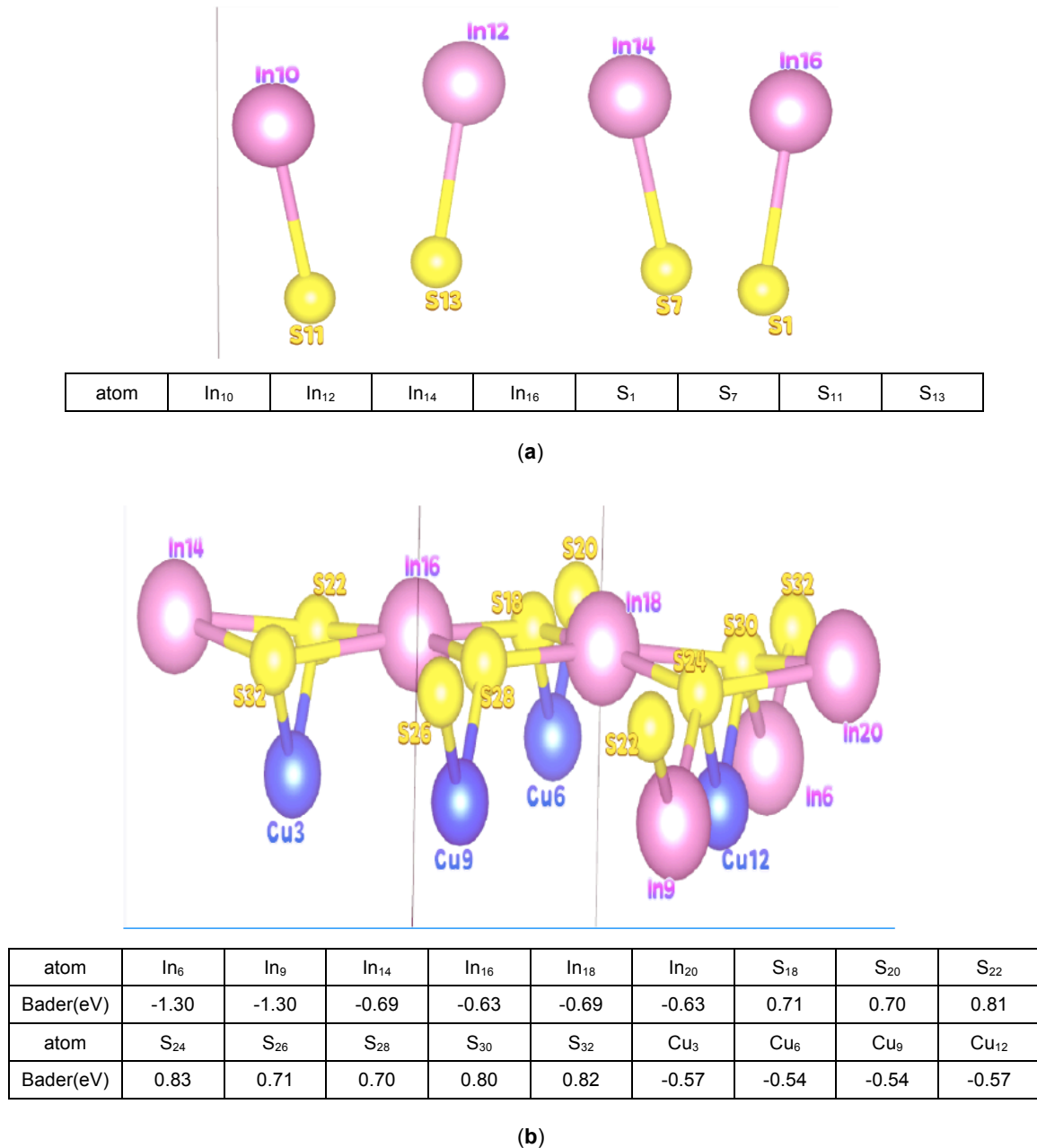


Figure 4: The Bader charge of some atoms at the interface of structure **a** and **b**.

electrons are transferred to the S atom in ZnIn_2S_4 , while the electrons lost by Cu and In in CuInS_2 material are also likely to be partially transferred to the S atom in ZnIn_2S_4 material. The other part is transferred to the S atom in the CuInS_2 material. By analyzing the differential charge density, electron local function and Bader charge of the structure, the results show that when the contact interface is different, the atoms exposed at the contact interface, the internal electric field generated and the electron transfer direction will be different, and the chemical bond is likely to be formed at the interface and the chemical action will be produced.

3.3. Band Structure

The band types of two-dimensional (2D) heterostructures are mainly divided into type I

(straddling type), type II (staggered type) and type III (broken type), and their structural characteristics are as follows:

Type I band structure: The two materials that make up the heterogeneous structure have overlapping conduction band minimum and valence band maximum. This means that electrons and holes can form electron-hole pairs in the same material layer, which facilitates the recombination and transport of charge carriers.

Type II band structure: The valence band maximum and conduction band minimum of one material are higher than that of another material respectively, and the valence band and conduction band of the two materials overlap respectively. In this structure, electrons and holes are confined to separate layers of

the material, which helps to improve the efficiency of carrier separation and reduce non-radiation.

Type III band structure: The valence band minimum of one material is higher than the conduction band maximum of the other material, and there is no overlap between the two. This structure is often metallic in nature. The band structure of type III heterostructures can be regulated by external conditions such as strain or chemical modification, which makes them have application potential in multi-functional devices.

The above three different types of heterojunction have different advantages and application potential in the field of electronics and optoelectronics.

In this study, the band edges of two 2D heterostructures were calculated by simulation software VASP (Vienna Ab-initio Simulation Package) based on density functional theory combined with the calculation results of the work function [40-42], as shown in Figure 5.

It can be seen from the band distribution that the valence band top of ZnIn_2S_4 material is lower than that of CuInS_2 material in structure a and b, while the conduction band bottom of ZnIn_2S_4 material is higher than that of CuInS_2 material. Therefore, both a and b belong to type I (straddling) heterostructures. For the heterostructure a, the energy required for electrons to transition from the valence band top of the ZnIn_2S_4 material to the conduction band bottom of the CuInS_2 material is 0.62eV. For heterostructure a, the energy released by the combination of ZnIn_2S_4 and CuInS_2 at the interface is 1.05eV, and 1.05eV is much larger than 0.6eV. Therefore, chemical bonds are most likely formed and chemical effects occur at the interface of heterostructure a. For heterostructure b, the energy

required for electrons to transition from the valence band top of ZnIn_2S_4 material to the conduction band bottom of CuInS_2 material is 1.05eV, and the energy required for electrons to transition from the valence band top of CuInS_2 material to the conduction band bottom of ZnIn_2S_4 material is 1.33eV. The energy released by ZnIn_2S_4 material and CuInS_2 material when combined at the interface is 4.47eV, which is much larger than 1.05eV and 1.33eV. Similarly, at the interface of heterostructure b, chemical bonds are most likely formed and chemical effects are generated.

Through the analysis of differential charge density, electron local function, Bader charge and band distribution of heterostructures a and b, the results show that chemical bond is formed at the interface of heterostructures a and b, and chemical interaction is generated, but not the interaction of van der Waals forces. This is because in structure a, the interface is exposed to the In atom in the ZnIn_2S_4 material and the S atom in the CuInS_2 material, and the S atom is very electronegative, so the electrons are transferred from the In atom in the ZnIn_2S_4 material to the S atom in the CuInS_2 material, and the In-S chemical bond is formed. For heterostructure b, the S atom in the material of ZnIn_2S_4 and the In and Cu atoms in the material of CuInS_2 are exposed at the interface. The electronegativity of the S atom is still very strong, so electrons are transferred from the In atom and Cu atom in the material of CuInS_2 to the S atom in the material of ZnIn_2S_4 , and formed In-S and Cu-S bonds. According to the electron local function, the chemical bonds formed between heterostructures a and b are ionic bonds. The contact between the ZnIn_2S_4 material and the CuInS_2 material creates a chemical interaction at the interface, and the chemical interaction at the interface causes the electrons inside the two materials

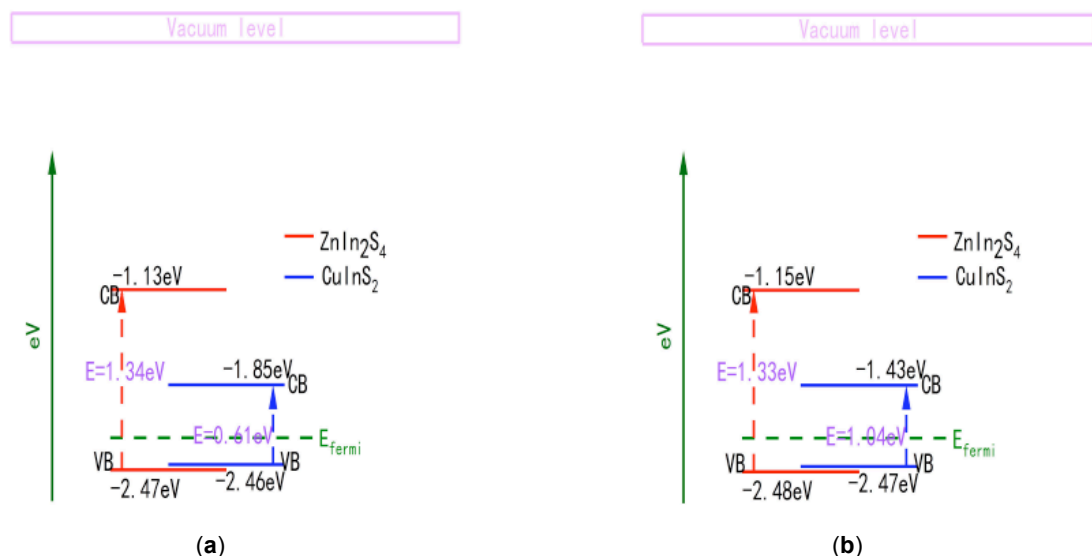


Figure 5: Band distribution of **a** and **b** structures.

to move. In addition, both a and b belong to type I (straddle) heterostructures, which makes heterostructures a and b form a quantum well at the interface, in which electrons and holes are confined to materials with lower energy bands and have advantages such as efficient luminescence characteristics, stronger carrier limitations, and tunable band structures. These advantages make heterostructures a and b of great application value in modern optoelectronics and microelectronics, especially in the development of high-performance light-emitting devices and photoelectric sensors.

3.4. Effective Mass

Effective mass refers to the inertial mass that a carrier exhibits as it moves through a solid, and is an equivalent concept used to describe the behavior of a carrier in an electromagnetic field. The effective mass [33] is the reciprocal of the radius of curvature of the carrier in the band structure, usually expressed by symbol m^* , the unit is kg or m_0 (mass of a free electron).

In this study, the effective mass is calculated using the un-weighted least square method by analyzing the dispersion relationship of the electron, that is, the relationship between the electron energy and the wave vector. In general, the dispersion relation of the band can be approximated by a quadratic polynomial near its minimum or maximum point, and the effective mass is directly related to the curvature of this quadratic polynomial [44]. The band structures of heterostructures a and b are calculated by band folding. In the calculation process, two high symmetric paths M→G and M→X are selected, and 9 points near the high symmetric point M are selected for fitting. The calculation formula is as follows:

$$E(k) = E_0 + \frac{\hbar^2}{2m^*} k^2 \quad (3)$$

where E_0 is the energy offset, m^* is the effective mass, \hbar is the reduced Planck constant, k is the wave vector. The calculated results are shown in Table 3, where M→G and M→X represent the effective mass of the carrier calculated along these two highly symmetric

directions, and a and b represent heterostructure a and heterostructure b. All the calculated results are based on the mass m_0 of the free electron.

The computed effective masses of electrons indicate a considerable discrepancy along the two symmetric routes, M→G and M→X, within the heterostructure a, and the effective mass of electrons in the highly symmetric path M→G is three times that in the highly symmetric path M→X, while the effective mass of holes in the two highly symmetric paths M→G and M→X is about the same. In the heterostructure b, the effective masses of electrons and holes in the two highly symmetric paths M→G and M→X are not very different. Moreover, both heterostructure a and heterostructure b have very small effective masses.

The migration of charge carriers, such as electrons or holes, within a semiconductor substance when subjected to an electrical field is termed carrier mobility. It is an important parameter to measure the electrical properties of semiconductor materials. It is usually represented by the symbol μ and the unit is $\text{cm}^2/(\text{V}\cdot\text{s})$. The higher the carrier mobility, the better the conductivity of the material. The relationship between carrier mobility and effective mass can be described by the classical drift diffusion equation as follows:

$$\mu = \frac{q\tau}{m^*} \quad (4)$$

where q is the charge of the carrier ($q=e$ for the electron and $q=-e$ for the hole). τ is the mean relaxation time of the carrier, that is, the average time for the carrier to move between the two collisions. m^* is the effective mass of the carrier. The formula shows that the carrier mobility is inversely proportional to the effective mass, and the smaller the effective mass, the higher the carrier mobility.

Therefore, the carriers in heterostructures a and b have high mobility and strong conductivity, so they are expected to become potential high-performance electronic devices, optoelectronic devices, thermoelectric materials, photocatalysis and energy storage materials.

Table 3: Carrier Effective Mass of Heterostructure a and b in M→G, M→X Direction

M → G				M → X			
a		b		a		b	
Electron(eV)	Hole(eV)	Electron(eV)	Hole(eV)	Electron(eV)	Hole(eV)	Electron(eV)	Hole(eV)
0.27	0.12	0.26	0.32	0.09	0.08	0.34	0.32

4. CONCLUSION

The basic physical properties of ZnIn₂S₄/CuInS₂ with different terminating heterostructures are calculated by first principles. The calculation results show that the binding energies of heterostructures a and b are -1.05eV and -4.47eV respectively, which indicates that both heterostructures a and b are stable and structure b is more stable. The calculated work function, differential charge density, electron localization function and bader charge show that for the heterostructure a, electrons are transferred from the In atom in the ZnIn₂S₄ material to the S atom in the CuInS₂ material. For heterostructure b, electrons are transferred from the In and Cu atoms in the CuInS₂ material to the S atoms in the ZnIn₂S₄ material. This shows that for 2D/2D heterostructures, the electron transfer direction will be different when the atoms exposed at the interface are different. Further calculation results of band structure show that both heterostructures a and b belong to type I (straddle) heterostructures, and heterostructure a forms In-S ionic bonds at the interface, and heterostructure b forms In-S ionic bonds and Cu-S ionic bonds at the interface. The results show that the carrier effective mass of heterostructures a and b is very small, which indicates that they are expected to be potential materials for high-performance electronic devices, optoelectronics, thermoelectric materials, photocatalysis and energy storage.

This study not only deepens the understanding of the basic physical properties of two-dimensional type I heterostructures, but also provides theoretical guidance for the optimal design of optoelectronic devices. The heterostructures revealed have important application value in the fields of high-performance light-emitting devices and photoelectric sensors. It is expected to inject new vitality into the research of two-dimensional materials.

DECLARATION OF COMPETING INTEREST

There are no conflicts to declare.

ACKNOWLEDGEMENTS

This work is supported by the National Natural Science Foundation of China Program (No.11164004, 61835003), the Guizhou Provincial Photonic Science and Technology Innovation team (Qianke Joint talents team [2015] 4017) and the First-class Physics Promotion Programme (2019) of Guizhou University.

REFERENCES

[1] Li, X.Y. Guo, X.M. Hu, W. Wang, Y.Y. Tai, M. Xie, Z. Li, S.L. Zhang, Realization of multifunction in perovskite-based van der Waals heterostructure by interface engineering strategy:

The case of CsPbBr₃/Janus MoSSe, *J. Appl. Surf. Sci.* 618 (2023) 156626.
<https://doi.org/10.1016/j.apsusc.2023.156626>

[2] Y. Kumar, R. Kumar, P.K. Raizadaa, A.A.P. Khanc, Q.Y. Van Le, P. Singha, V.H. Nguyene, Novel Z-Scheme ZnIn₂S₄-based photocatalysts for solar-driven environmental and energy applications: Progress and perspectives, *J. J. Mater. Sci. Technol.* 87 (2021) 234-257.
<https://doi.org/10.1016/j.jmst.2021.01.051>

[3] H.R. Zhang, M.Y. Cui, Y.J. Lv, Y.F. Rao, Y. Huang, A short review on research progress of ZnIn₂S₄-based S-scheme heterojunction: Improvement strategies, *J. Chinese Chem Lett.* 2024 110108.
<https://doi.org/10.1016/j.ccllet.2024.110108>

[4] G.P. Zhang, H. Wu, D.Y. Chen, N.J. Li, Q.F. Xu, H. Li, J.H. He, J.M. Lu, A mini-review on ZnIn₂S₄-Based photocatalysts for energy and environmental application, *J. GEE.* 7 (2022) 176-204.
<https://doi.org/10.1016/j.gee.2020.12.015>

[5] J. Wang, S.J. Sun, R. Zhou, Y.Z. Li, Z.T. He, H. Ding, D.M. Chen, W.H. Ao, A review: Synthesis, modification and photocatalytic applications of ZnIn₂S₄, *J. Mater. Sci. Technol.* 78 (2021) 1-19.
<https://doi.org/10.1016/j.jmst.2020.09.045>

[6] M.Q. Xu, R. Zhang, J. He, Z.Y. Chen, J.C. Jiang, Z.X. Li, Y.J. Liu, D. Chen, Y.H. Ma, Construction of heterojunctions with in situ growth of ZnIn₂S₄ nanosheets on the surface of atomically dispersed Cu-modified MOFs for high-performance visible-light photocatalytic antibiotic degradation, *J. Sep Purif Technol.* 354 (2025) 129093.
<https://doi.org/10.1016/j.seppur.2024.129093>

[7] X. Wang, N. Zhang, F. Zhao, X.C. Zhang, W.L. Wu, Y.H. Wang, Hollow Zn_{0.01}Co_{0.99}Se₂/ZnIn₂S₄ Z-scheme heterogeneous photocatalyst with Strong internal electric field and Excellent surface electron transfer capability for Efficient Hydrogen Production, *Ceram Int.* 49 (2023) 30744-30754.
<https://doi.org/10.1016/j.ceramint.2023.07.030>

[8] S.T. Liu, L. Wu, L.S. Zhao, A photoelectrochemical platform constructed with C-doped ZnIn₂S₄/Bi₂S₃: Excellent for the visual detection of tumor marker, *Electrochim Acta.* 491 (2024) 144328.
<https://doi.org/10.1016/j.electacta.2024.144328>

[9] L.G. Ma, Y.H. Ding, C. Lin, Y.Q. Yang, L. Xu, H. Qiu, H.L. Jiang, X. Song, X.Q. Ai, ZnIn₂S₄ nanostructure grown on electronegative h-BN for highly efficient photocatalytic hydrogen evolution, *Int J Hydrogen Energ.* 83 (2024) 553-562.
<https://doi.org/10.1016/j.ijhydene.2024.08.132>

[10] X.J. Feng, H.S. Shang, J.L. Zhou, X.K. Ma, X.Y. Gao, D. Wang, B. Zhang, Y.F. Zhao, Heterostructured core-shell CoS_{1.097}@ZnIn₂S₄ nanosheets for enhanced photocatalytic hydrogen evolution under visible light, *Chem. Eng. J.* 457 (2023) 141192.
<https://doi.org/10.1016/j.cej.2022.141192>

[11] H.L. Ding, Y.X. Feng, Y.F. Xu, X.D. Xue, R. Feng, T. Yan, L.G. Yan, Q. Wei, Self-powered photoelectrochemical aptasensor based on MIL-68(In) derived In₂O₃ hollow nanotubes and Ag doped ZnIn₂S₄ quantum dots for oxytetracycline detection, *Talanta.* 240 (2022) 123153.
<https://doi.org/10.1016/j.talanta.2021.123153>

[12] M. Zhang, M. Arif, Y.Y. Dong, X.B. Chen, X.H. Liu, Z-scheme TiO_{2-x}@ZnIn₂S₄ architectures with oxygen vacancies-mediated electron transfer for enhanced catalytic activity towards degradation of persistent antibiotics, *J. Colloid Surface A.* 649 (2022) 129530.
<https://doi.org/10.1016/j.colsurfa.2022.129530>

[13] L.L. Kazmerski, M.S. Ayyagari, G.A. Sanborn, CuInS₂ thin films: Preparation and properties, *J. Appl. Phys.* 46 (1975) 4865-4869.
<https://doi.org/10.1063/1.321521>

[14] K.O. Joanna, W. Horst, Synthesis and Application of Colloidal CuInS₂ Semiconductor Nanocrystals, *J. ACS Appl. Mater. Interfaces.* 5 (2013) 12221-12237.
<https://doi.org/10.1021/am404084d>

- [15] S. Kaowphongsa, W. Choklapa, A. Chachvalvutikula, N. Chandeta, A novel $\text{CuInS}_2/\text{m-BiVO}_4$ p-n heterojunction photocatalyst with enhanced visible-light photocatalytic activity, *J. Colloid Surface A*. 579 (2019) 123639. <https://doi.org/10.1016/j.colsurfa.2019.123639>
- [16] Z.J. Guan, J.W. Pan, Q.Y. Li, G.Q. Li, J.J. Yang, Boosting Visible-Light Photocatalytic Hydrogen Evolution with an Efficient $\text{CuInS}_2/\text{ZnIn}_2\text{S}_4$ 2D/2D Heterojunction, *J. ACS Sustainable Chem. Eng.* 7 (2019) 7736-7742. <https://doi.org/10.1021/acssuschemeng.8b06587>
- [17] X.K. Xiang, M. Zhang, Q.T. Huang, Y. Mao, J.H. Jia, X.T. Zeng, Y.Y. Dong, J.M. Liao, X.B. Chen, X.X. Yao, Q.F. Zheng, W. Chen, Construction of S-scheme $\text{CuInS}_2/\text{ZnIn}_2\text{S}_4$ heterostructures for enhanced photocatalytic activity towards Cr(VI) removal and antibiotics degradation, *J. Chemosphere*. 352 (2024) 141351. <https://doi.org/10.1016/j.chemosphere.2024.141351>
- [18] V.V. Bozhko, A.V. Novosad, G.E. Davidiyuk, V.R. Kozler, O.V. Parasyuk, N. Vainorius, V. Janonis, A. Sakavic, A. Sakavicius, V. Kazukauskas, Electrical and photoelectrical properties of $\text{CuInS}_2\text{-ZnIn}_2\text{S}_4$ solid solutions, *J. Alloy Compd.* 553 (2013) 48-52. <https://doi.org/10.1016/j.jallcom.2012.10.134>
- [19] F.Y. Li, B.Y. Liao, J.N. Shen, J.N. Ke, R.X. Zhang, Y.Q. Wang, Y. Niu, Enhancing Photocatalytic Activities for Sustainable Hydrogen Evolution on Structurally Matched $\text{CuInS}_2/\text{ZnIn}_2\text{S}_4$ Heterojunctions. *J. Molecules*. 29 (2024) 2447. <https://doi.org/10.3390/molecules29112447>
- [20] B. Diola, Understanding density functional theory (DFT) and completing it in practice, *J. AIP Adv.* 4 (2014) 127104. <https://doi.org/10.1063/1.4903408>
- [21] K. Burke, L. O. Wagner, DFT in a Nutshell, *Int J Quantum Chem.* 113 (2013) 30744-30754. <https://doi.org/10.1002/qua.24411>
- [22] V. Wang, N. Xu, J. C. Liu, G. Tang, W.T. Geng, VASPKit: A User-Friendly Interface Facilitating High-Throughput Computing and Analysis Using VASP Code, *Comput Phys Comm.* 267 (2021) 108033. <https://doi.org/10.1016/j.cpc.2021.108033>
- [23] S.Q. Liu, Y.B. Li, Z.M. Yang, H.Q. Tian, J.M. Liu, Reduced partition function ratios of iron, magnesium, oxygen, and silicon isotopes in olivine: A GGA and GGA + U study, *J. Geochim Cosmochim Acta.* 384 (2024) 111-127. <https://doi.org/10.1016/j.gca.2024.09.017>
- [24] M.A. Majeed Khana, S. Kumarb, M.S. Alsahlia, M. Ahameda, M. Alhoshana, S.A. Alrokayana, T. Ahamade, Morphology and non-isothermal crystallization kinetics of CuInS_2 nanocrystals synthesized by solvo-thermal method, *J. Mater Charact.* 65 (2012) 109 - 114. <https://doi.org/10.1016/j.matchar.2012.01.009>
- [25] J.A.F. Ramos, V. Soto, J.A.L. Ceron, M.O.V. Lepe, R.F. Moreno, Measurement of core electron binding energies of silver nanoparticles and their modeling with electron propagator calculations of silver clusters, *J. Inorg Chim Acta*, 573 (2024) 122338. <https://doi.org/10.1016/j.ica.2024.122338>
- [26] A. Kachu, S. Vemula, N.R. Chebrolu, A. Boda, Role of confinement shape and spin-orbit interactions on binding energy, temperature, transition energy, susceptibility and oscillator strength of an off-center D^0 impurity in a GaAs quantum dot, *J. Physica B*, 693 (2024) 416376. <https://doi.org/10.1016/j.physb.2024.416376>
- [27] H. Lu, J.T. Yu, Q.W. Zhang, J.A. Zhang, C. Zhang, Q.Y. Bi, Data-driven deep learning prediction of boron-doped graphene work function, *J. Mater Today Commun*, 40 (2024) 109924. <https://doi.org/10.1016/j.mtcomm.2024.109924>
- [28] Y.T. Chen, Q. Sun, Z.G. Ni, X.W. Tu, C. Sun, S.X. Zhu, X.F. Duan, M. Jiang, Z.J. Xie, M. Liu, H. Zheng, High-efficient solar-driven nitrogen fixation by modulating the internal electric-field of MOFs via n-site-enhanced charge density difference in organic ligands, *Chem Eng J*, 482 (2024) 148853. <https://doi.org/10.1016/j.cej.2024.148853>
- [29] M. Wolloch, G. Levita, P. Restuccia, M.C. Righi, Interfacial Charge Density and Its Connection to Adhesion and Frictional Forces, *J. Phys. Rev. Lett.* 121 (2018) 026804. <https://doi.org/10.1103/PhysRevLett.121.026804>
- [30] B.J. Ransil, J.J. Sinai, Toward a Charge-Density Analysis of the Chemical Bond: The Charge-Density Bond Model, *J. Chem. Phys.* 46 (1967) 4050-4074. <https://doi.org/10.1063/1.1840487>
- [31] R.F. Nalewajski, A.M. Koster, S. Escalante, Electron Localization Function as Information Measure, *J. Phys. Chem.* 109 (2005) 10038-10043. <https://doi.org/10.1021/jp053184i>
- [32] T. Lu, F.W. Chen, Meaning and Functional Form of the Electron Localization Function, *J. Acta Phys. Chim. Sin.* 27 (2011) 2786-2792. <https://doi.org/10.3866/PKU.WHXB20112786>
- [33] M. Kohout, F.R. Wagner, Y. Grin, Electron localization function for transition-metal compounds, *J. Theor Chem Acc.* 108 (2002) 150-156. <https://doi.org/10.1007/s00214-002-0370-x>
- [34] J. Poater, M. Duran, M. Sola, B. Silvi, Theoretical Evaluation of Electron Delocalization in Aromatic Molecules by Means of Atoms in Molecules (AIM) and Electron Localization Function (ELF) Topological Approaches, *J. Chem. Rev.* 105 (2005) 3911-3947. <https://doi.org/10.1021/cr030085x>
- [35] M. Yu, D.R. Trinkle, Accurate and efficient algorithm for Bader charge integration, *J. Chem. Phys.* 134 (2011) 064111. <https://doi.org/10.1063/1.3553716>
- [36] N.M. Rasi, S. Ponnurangam, N. Mahinpey, First-principles investigations into the effect of oxygen vacancies on the enhanced reactivity of NiO via Bader charge and density of states analysis, *J. Catal. Today.* 407 (2023) 172-181. <https://doi.org/10.1016/j.cattod.2022.01.012>
- [37] S. Aii, P.M. Ismail, H.H. Shen, A. Zada, A. Ali, I. Ahmad, R. Shah, I. Khan, J.S. Chen, C.H. Cui, X.Q. Wu, Q.Q. Kong, J.B. Yi, X.T. Zu, H.Y. Xiao, F.Z. Raziq, L. Qiao, Synthesis and bader analyzed cobalt-phthalocyanine modified solar UV-blind $\beta\text{-Ga}_2\text{O}_3$ quadrilateral nanorods photocatalysts for wide-visible-light driven H_2 evolution, *J. Appl. Catal., B-Environ.* 307 (2022) 121149. <https://doi.org/10.1016/j.apcatb.2022.121149>
- [38] S. Barnetta, D. Allana, M. Gutmann, J.K. Cockcroft, V.H. Maid, A.E. Aliev, J. Saßmannshausen, Combined high resolution X-ray and DFT Bader analysis to reveal a proposed Ru-H-Si interaction in $\text{Cp}(\text{IPr})\text{Ru}(\text{H})_2\text{SiH}(\text{Ph})\text{Cl}$, *Inorg Chem Aata.* 488 (2019) 292-298. <https://doi.org/10.1016/j.ica.2019.01.034>
- [39] H.P. Beck, A DFT study on the correlation between topology and Bader charges: Part V, on the correlation between interatomic distances and Bader charges in the structures of Ti_nO_m compounds A comment on the "charge and size concept" in crystal chemistry, *J. Solid State Sci.* 67 (2017) 85-92. <https://doi.org/10.1016/j.solidstatesciences.2017.03.010>
- [40] Q.S. Zeng, H. Wang, W. Fu, Y.J. Gong, W. Zhou, P.M. Ajayan, J. Lou, Z. Liu, Band Engineering for Novel Two-Dimensional Atomic Layers, *J. 2D Mater.* 16 (2015) 1868-1884. <https://doi.org/10.1002/sml.201402380>
- [41] T.A. Shifa, F.M. Wang, Y. Liu, J. He, Heterostructures Based on 2D Materials: A Versatile Platform for Efficient Catalysis, *J. Adv. Mater.* 31 (2019) 1804828. <https://doi.org/10.1002/adma.201804828>
- [42] T.M. Su, Z.D. Hood, M. Naguib, L. Bai, S. Luo, C.M. Rouleau, N. Ivanov, H.B. Ji, Z.Z. Qin, Z.L. Wu, 2D/2D heterojunction of $\text{Ti}_3\text{C}_2/\text{g-C}_3\text{N}_4$ nanosheets for enhanced photocatalytic hydrogen evolution, *J. Nanoscale.* 11 (2019) 8051-8628. <https://doi.org/10.1039/C9NR90098E>
- [43] Y. Yua, H.D. Xiong, K. Eshuna, H. Yuan, Q.L. Li, Phase transition, effective mass and carrier mobility of MoS_2 monolayer under tensile strain, *J. Appl Surf Sci*, 325 (2015) 27-32. <https://doi.org/10.1016/j.apsusc.2014.11.079>

[44] A. Raghav, K. Hongo, R. Maezono, E. Panda, Electronic structure and effective mass analysis of doped TiO_2 (anatase) systems using DFT+U, J. Comp Mater Sci, 214

(2022) 111714.

<https://doi.org/10.1016/j.commatsci.2022.111714>

Received on 08-04-2025

Accepted on 20-05-2025

Published on 27-05-2025

<https://doi.org/10.31875/2410-2199.2025.12.04>

© 2025 Wang *et al.*

This is an open-access article licensed under the terms of the Creative Commons Attribution License (<http://creativecommons.org/licenses/by/4.0/>), which permits unrestricted use, distribution, and reproduction in any medium, provided the work is properly cited.